Journal of the European Ceramic Society 20 (2000) 1611–1620

Electrical transport properties in zirconia/alumina functionally graded materials

A.J. Sánchez-Herencia*, R. Moreno, J.R. Jurado

Instituto de Cerámica y Vidrio, CSIC, Crtra. Valencia Km. 24,300, 28500 Arganda del Rey, Madrid, Spain

Received 17 May 1999; received in revised form 5 August 1999; accepted 8 August 1999

Abstract

Functionally graded materials (FGMs) are promising candidates for the fabrication of technological components, not only as structural devices, but also in electrochemical ones, such as solid oxide fuel cells (SOFC), or high-efficiency hybrid direct energy conversion systems. In the present work FGMs were prepared by the sequential slip casting technique, starting with an yttria tetragonal zirconia polycrystalline layer and increasing subsequently the amount of Al_2O_3 in the following layers. Electrochemical impedance spectroscopy (EIS) analysis was used to evaluate the electrical characteristics of these materials and to compare with those of the monolithic compacts. In general, it was observed that the FGM conductivity is ruled by the conductivity of the layer which contains the highest amount of alumina blocking particles. By EIS no electrical interfaces between adjoining layers were detected and, accordingly, no specific electric ohmic losses were observed. The conductivity of the FGMs is close to that calculated using the normalized thicknesses and the alumina volume fractions of the layers after measuring the conductivity of the monolithic materials with the same composition to what correspond to that of the final layer in the FGM. These results suggest that the gradient structure can be used to control the oxygen vacancy motion, and then applied in electrochemical devices.

Keywords: Functionally graded materials; Slip casting; Al_2O_3–ZrO_2; Composites; Impedance spectroscopy; Ionic conductivity

1. Introduction

Functionally graded materials (FGMs) are materials in which certain properties change continuously from one surface to the other. The preparation of FGMs has been performed by a wide number of techniques related to both ceramics and metal processing and have been widely discussed in the international meetings on this subject[1,2,3] and summarized in some papers[4] and books.[5] The main requirement for these techniques is to achieve any desired composition profile to face the designed properties in the material.

After the pioneer works on FGMs for structural applications as thermal barrier coatings and stress relief materials, more uses have been worked out, mostly focused on electronic and functional applications. The FGM concept has been used to produce actuator devices where the graded materials behave better than bimorph actuators in thermal resistance, peeling resistance and reliability[6] due to the absence of bonding agents. It also allows the fabrication of materials with elliptic movement.[7] Another electrical application of FGMs is the design of a high-efficiency hybrid direct energy conversion system (HYDECS) using direct heat for electricity convertor materials, which may provide a conversion efficiency above 40% from a nuclear or solar source with a heat sink temperature of 300 K.[8,9] In the solid oxide fuel cells (SOFC) field the FGM concept has been proposed for the development of materials with lower thermal stresses[10] and systems in which the reactivity and ohmic losses between cathode and solid electrolyte[11,12] could be eliminated.

Emerging technologies are demanding new materials, composites or not, with electrical multifunction properties, enhancing other structural performances, such as mechanical and thermal expansion matching. Ceramic FGMs satisfy this requirement. Despite of these emerging applications, not many studies have been presented in the literature regarding to the electrical properties of those FGMs.[13]

* Corresponding author. Tel.: +34-91-871-1800; fax: +34-91-870-0550.

E-mail address: ajsanchez@icv.csic.es (A.J. Sánchez-Herencia).

0955-2219/00/$ - see front matter
PII: S0955-2219(99)00215-0

It has been demonstrated that electrochemical impedance spectroscopy (EIS)[14] is an accurate, non-destructive technique for the characterization of bulk materials, and other unspecific phases, as secondary phases, porosity, cracks, etc.[15–17] New equations have been established which allow a more quantitative analysis of the impedance/admittance diagrams. Using this tool some electrical properties of zirconia/alumina composites can be examined. For instance, in yttria-stabilized zirconia (YSZ) the research have been mostly focused on small additions of a secondary phase in order to improve the mechanical properties of the solid electrolyte.[18,19] In all cases, a regular increase in the grain boundary resistance has been observed. It is generally interpreted in terms of a grain boundary surface increase with increasing alumina additions. The experimental results that have been previously reported[18,20] have convincingly shown that microstructure blockers (alumina particles, cracks, pores, etc.) generate blocking effects which relax at variable frequencies depending on their average dimension parallel to the currentline direction.

In the present work, layered FGMs have been obtained by sequential slip casting which allows the fabrication of controlled composition and thickness of each layer.[6] Several layered FGMs have been made by this technique in the system Al_2O_3/ZrO_2 and their electrical characteristics have been studied using EIS.

2. Experimental procedure

The starting powders were high purity (99.99%) commercial Al_2O_3 and yttria tetragonal zirconia polycrystalline (Y-TZP). Table 1 shows the main characteristics of these two powders.

From these powders, pure Al_2O_3 and Y-TZP slips were prepared to solid content of 70 wt.%. The pH of the alumina slurry was adjusted to 4, while the pH of the zirconia slip was not changed because direct mixing in water provided a pH value of 5.6 where the viscosity was low enough for the casting process. Those slurries were ball milled in an alumina jar mill using alumina balls. In order to prepare the mixture compositions, the stable pure material slurries were blended in the proper ratios to obtain six intermediate slurries named 15A, 30A, 45A, 55A, 70A and 85A, the numbers meaning the concentration of alumina (in wt.%) in the mixture. No subsequent pH adjustments were made in the mixtures.[21] The pure zirconia (Y-TZP) and alumina slurries were labeled 0A and 100A, respectively.

Table 1
Characteristics of the starting powders

	Purity (wt.%)	Density (g/cm^3)	D_{50} (μm)	S_s (m^2/g)
Al_2O_3 (Condea, HPA 0.5)	99.99	3.88	0.3	9.5
Y-TZP (Tosoh, TZ-3YS)	99.98	5.81	0.4	6.7

Table 2
Definition of layers sequence in the prepared functionally graded materials (FGMs)

Material	Layers sequence
FGM-100	0A/15A/30A/45A/55A/70A/85A/100A
FGM-85	0A/15A/30A/45A/55A/70A/85A
FGM-70	0A/15A/30A/45A/55A/70A
FGM-55	0A/15A/30A/45A/55A
FGM-45	0A/15A/30A/45A

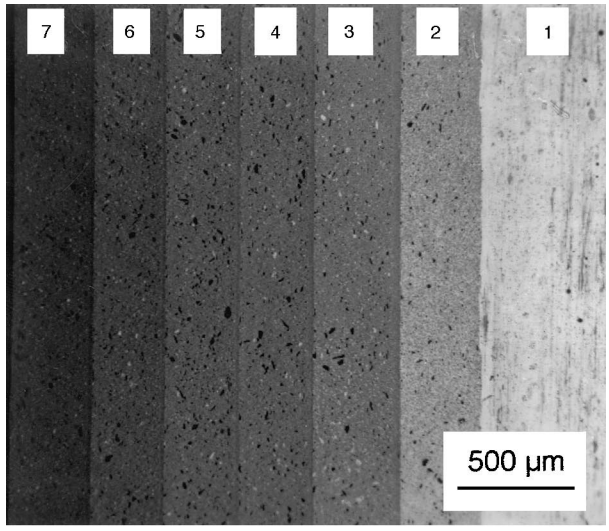

(a)

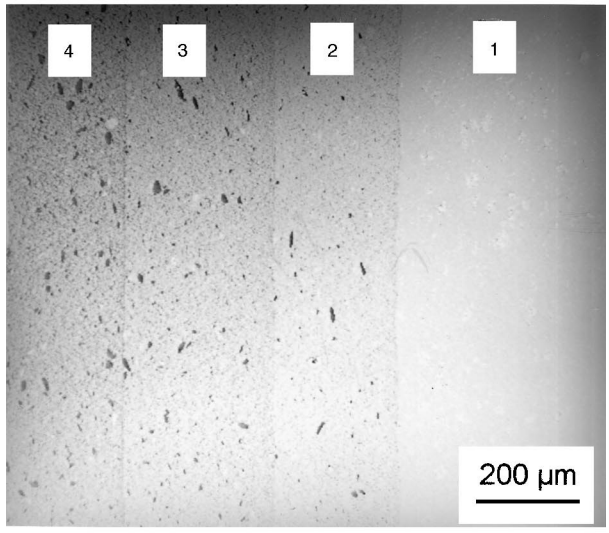

(b)

Fig. 1. General SEM micrographs of functionally graded materials (FGMs) with (a) seven and (b) four layers. (Numbers 1, 2, 3, 4, 5, 6 and 7 correspond with 0A, 15A, 30A, 45A, 55A, 70A and 85A, respectively).

The slips were sequentially cast onto plaster of Paris molds in order to prepare the FGMs containing eight layers of compositions varying from Y-TZP to Al_2O_3. The 0A wall thickness formation rate was used to calculate the casting time of each slurry for the preparation of the materials with layers of 200–300 μm thickness each. In all cases the starting layer in the laminated FGM was the 0A composition. Five different layered structures were designed from the starting FGM with eight layers by suppressing one layer in each case up to the fabrication of a FGM with only four layers varying from 0A to 45A. Table 2 shows the internal composition for the five cast FGMs. Materials with less amount of layers could not be obtained since they broke during removal from the casting mold because of their low thickness.

Other than the different FGMs, also monolithic composite materials of Al_2O_3/Y-TZP with compositions of 100A, 85A, 70A, 55A, 45A, 30A, 15A and 0A were prepared. These monolithic compacts were cast in cylindrical shaped molds of 7 mm diameter.

Green materials were sintered in air at 1550°C for 2 h with a heating/cooling rate of 5°C/min. The sintered FGMs were cut in squared specimens of 10 mm width and the monolithics were cut in 1 mm slides. Sintered samples were polished using diamond paste down to 1 μm and thermally etched at 1450°C (1 h) for microstructural observations by scanning electron microscopy (SEM).

As electrodes, high conductivity platinum paste was applied onto both sides of the sample, parallel to the layers. It was heat-treated at 900°C for 10 min. The impedance spectroscopy analysis EIS was used to characterize all materials investigated, in the frequency range of 10–10^6 Hz, and at temperatures from 300 to 1000°C, in air, by using an impedance analyzer HP4192A. A two-electrode assembly located in a hot-sample holder with temperature control was used. The impedance spectra were mathematically analyzed using commercial software EQUIVCRT.[22]

Table 3
Measured thickness of each layer in each functionally graded materials (FGMs)

Sample	Layer's thickness (μm)								Total (mm)
	0A	15A	30A	45A	55A	70A	85A	100A	
FGM-100	346	224	328	259	259	233	233	233	2.1
FGM-85	522	306	340	295	295	295	295		2.35
FGM-70	493	288	300	298	298	298			1.98
FGM-55	540	300	300	300	300				1.74
FGM-45	500	290	305	295					1.39

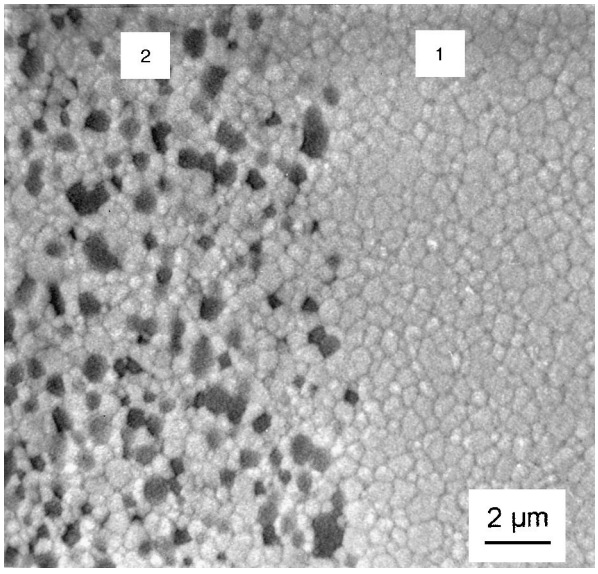

Fig. 2. SEM microstructure of the interface between layers of pure tetragonal zirconia polycrystalline (TZP) (0A) and 15A in the eight-layers functionally graded materials (FGM).

3. Results

3.1. Microstructural characterization

Fig. 1 shows a general view of the graded materials with four and seven layers. Table 3 shows the final thickness of each layer as directly measured on the micrographs for all studied graded materials. As can be observed, the thickness of the first layer (Y-TZP) is higher in all cases, as a consequence of the sigmoidal casting kinetics. At the beginning of the process, the

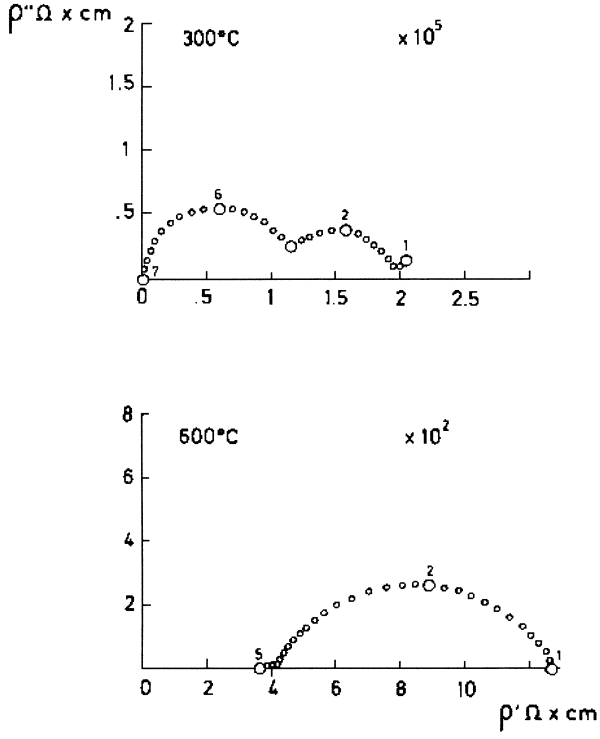

Fig. 3. Impedance spectrum of monolithic sample 0A [pure tetragonal zirconia polycrystalline (TZP)] at 300 and 600°C.

error in time measurements, mainly due to the filling and pouring out of the mold, generates large errors in the thickness. After this first step, the other layers show more uniform thickness ranging between 200 and 300 μm as predicted. Isolated black dots are observed in the micrographs, corresponding to small agglomerated regions (5–10 μm) of alumina where no second phase was presented. Because of its low quantity and small size, these agglomerated regions were considered not to have influence on the overall electrical properties.

Fig. 2 shows the 0A/15A interface in the FGM with eight layers. No delamination was observed in any case and the interfaces between adjoining layers are very narrow (less than one micron) and well defined. The density was closer to the theoretical and only remaining porosity could be observed in the layers with high alumina content for both the monolithics and the graded materials. The dispersion and homogeneity of the phases is very high as a result of a colloidal method. The grain size of alumina was measured over the SEM micrograph. It was observed that pure alumina layer has a mean size of 4 μm; the layer called 85A has a grain size of 2 μm and the other layers have a homogeneous mean size of 0.5 μm approximately for the alumina grains. In the 15A layer the grain size distribution of alumina was narrower.

3.2. Electrical EIS measurements on FGM materials

The general electrochemical cell for all the EIS measurements is:

air, Pt//XXX//Pt, air

where XXX can be a monolithic material or a layered FGM. For example, in the FGM-100 the electrochemical cell is:

air, Pt//0A/15A/30A/45A/55A/70A/85A/100A//Pt, air

Electrical measurements were performed in parallel for the monolithic compacts and the FGMs for comparison purposes.

Fig. 3 shows the impedance spectrum of the sample 0A (pure-TZP material), at 300°C in which two clear arcs are seen. All the data are normalized to a geometrical factor equal to 1. The high frequency arc corresponds to the bulk conductivity contribution, and the

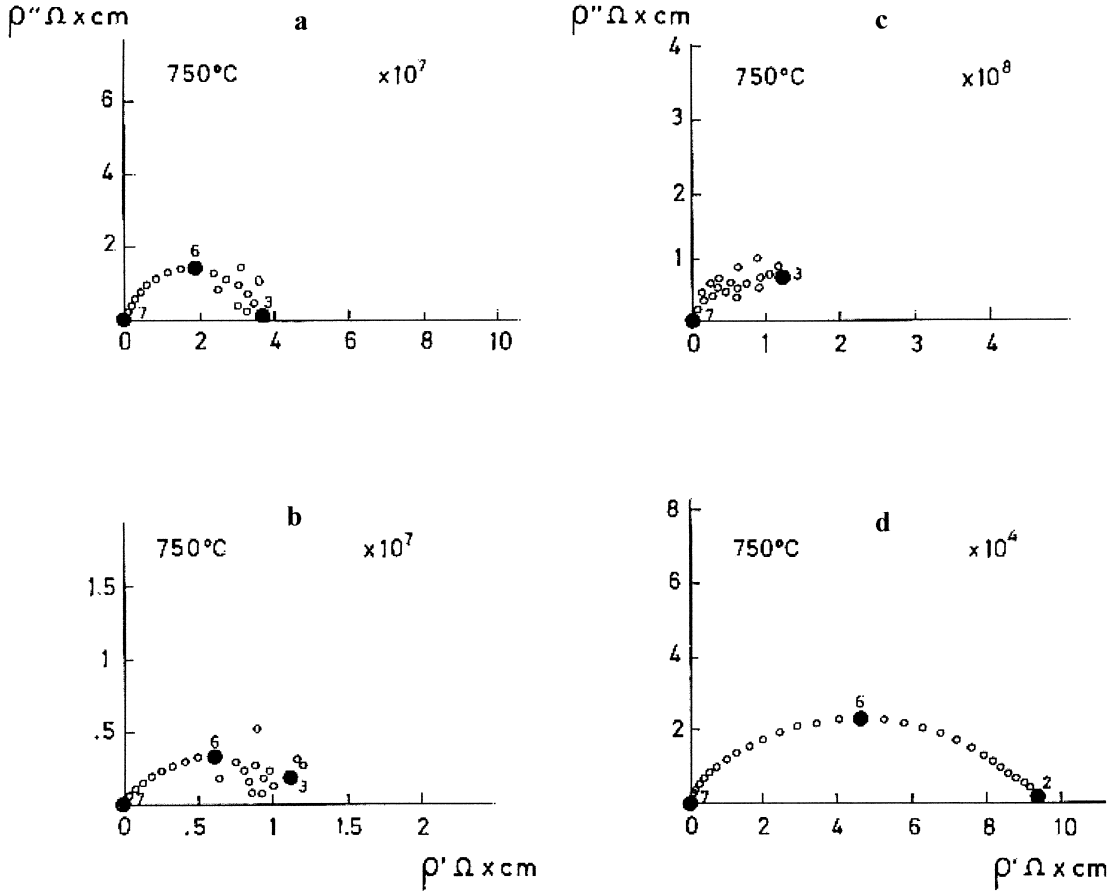

Fig. 4. Impedance spectra of monolithic materials of composition (a) 100A and (b) 85A, and of functionally graded materials (FGMs) whose last layer have compositions (c) 100A and (d) 85A.

intermediate frequency arc is ascribed to grain boundary conduction contribution. When temperature is raised up to 600°C, the bulk contribution to the relaxation process disappears, and the Pt/TZP electrode interface is then registered. At temperatures higher than 600°C only a small semicircle appears, fully associated to that interface. This pure $Zr(Y)O_2$ layer is present in all the FGM materials, being the thickest one. The higher thickness of this layer in all cases will not interfere with the results due to the very high conductivity of this composition at the studied temperatures.

Fig. 4 shows the impedance spectra of monolithic materials with compositions 100A (Fig. 4(a)) and 85A (Fig. 4(b)) and the spectra of the FGMs whose final layer have compositions 100A (Fig. 4(c)) and 85A (Fig. 4(d)). The monolithic alumina behaves as an insulator, as expected. In the sample FGM-100, the presence of an insulating layer 100A blocks all the mobile ions and the impedance spectrum at temperatures as high as 750°C, shows that the conductivity is 1.0×10^{-8} S/cm. Therefore, the FGM-100 is still considered as an insulator in the perpendicular direction to the layers. A surprising observation from these spectra is that the conductivity of monolithic alumina is higher than that of the FGM with only a thin layer of 100A, contrary to the expected behavior.

In the case of sample FGM-85, the insulating layer 100A was suppressed and the impedance spectrum shows a semicircle almost clear from 300°C. The conductivity of this sample at 750°C is 1.0×10^{-5} S/cm, just three orders of magnitude higher to that of FGM-100 (1.0×10^{-8}). On the other hand, the conductivity of the FGM-85 is also three orders of magnitude higher than that of the monolithic 85A (8.4×10^{-8} S/cm). The different behavior found for these samples must be related to their different total concentration of alumina in the whole material, being around 90 vol.% in the monolithic versus 45 vol.% in the FGM.

The FGM-70, was prepared by suppressing the 100A and the 85A layers. Fig. 5 shows the impedance spectrum

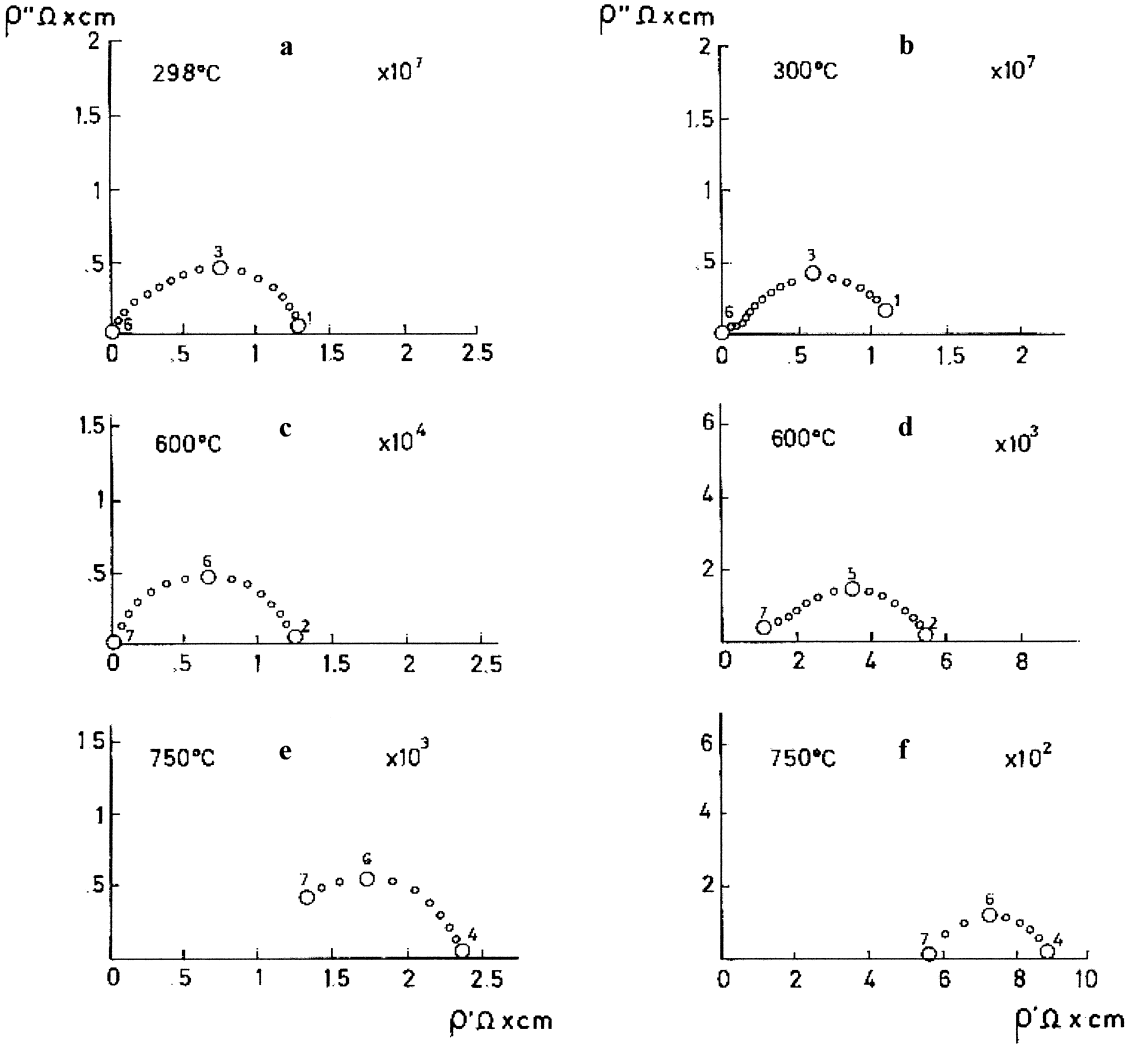

Fig. 5. Impedance spectra of monolithic materials with composition ((a), (c) and (e)) 70A and of ((b), (d) and (f)) functionally graded materials (FGM)-70 at different temperatures.

of both monolithic of 70A (Figs. 5(a), (c) and (e)) and FGM-70 (Figs. 5(b), (d) and (f)) at different temperatures. At 300°C two overlapped arcs can be detected in the FGM-70 while the spectra of the 70A monolithic sample can be deconvoluted in two different arcs. The high frequency small arc can be associated to the bulk oxygen vacancy conduction of the TZP phase, since the measured conductivity is 1.1×10^{-6} S/cm. The pure-TZP bulk conductivity is around eight times higher. This suggests that the bulk conductivity is modified by the alumina blocking effect, in the same way that was reported by Kleitz and Steil.[17] The low frequency semicircle seems to be related to the overall blocking effect of the microstructure defects: regular grain boundaries of Y-TZP and alumina inclusions. The depression angle in this region is rather high ($\omega = 14°$). At 600°C the small arcs disappear and the second arcs also shift up ($\omega = 18°$). The conductivity of the FGM-70 is also large 1.8×10^{-4} S/cm in relation to that of monolithic 70A. In this case the total alumina concentration is around 38 vol.% in the FGM and near 80 vol.% in the monolithic 70A. A slight deformation appears at this temperature, near the high frequency which must be related to the blocking effect caused by microstructural defect.[23] At higher temperature (750°C) this arc deformation completely disappears suggesting that the Pt/FGM-70 interface is mainly responsible for this frequency displacement. Similar observations were found for the monolithic material.

FGM-55 is obtained when layers 100A, 85A and 70A are suppressed. Fig. 6 plots the impedance spectra at

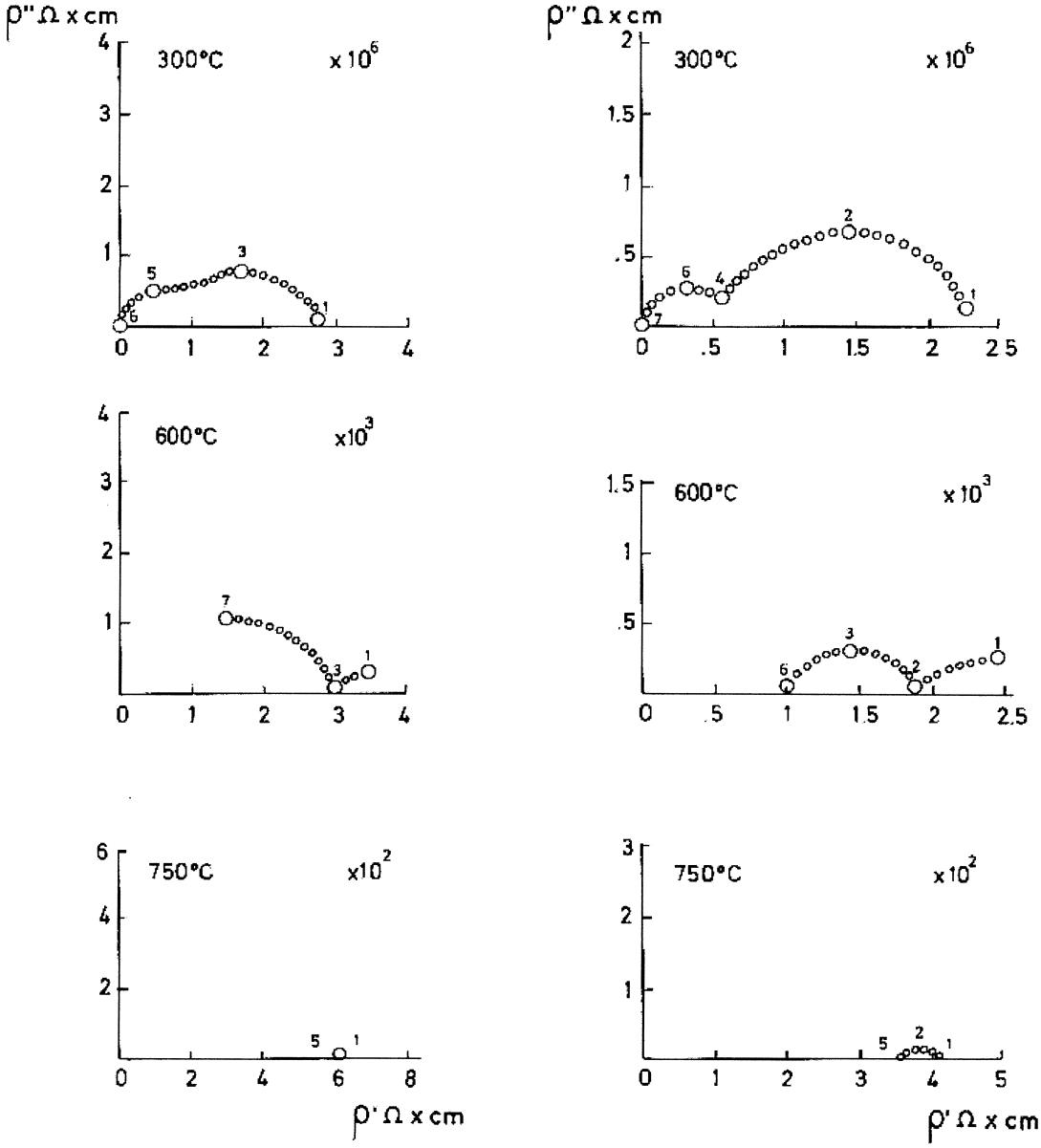

Fig. 6. Impedance spectra of monolithic materials with composition ((a), (c) and (e)) 55A and of ((b), (d) and (f)) functionally graded materials (FGM)-55 at different temperatures.

different temperatures for the monolithic 55A material (Fig. 6(a), (c) and (e)) and for the FGM-55 (Fig. 6(b), (d) and (f)). The spectra obtained for FGM-45 in which four layers were eliminated can be observed in Fig. 7(a), (b) and (c), corresponding to measurements performed at 300, 600 and 750°C.

Both FGM composites present quite similar spectra with the same arc shape and morphology at the same temperature. Slight deviations in the total conductivity values are appreciated, but always in the same range. At 300°C two arcs are observed, and the total conductivities are 4.3×10^{-7} and 5.0×10^{-7} S/cm for FGM-55 and FGM-45, respectively. These values are slightly higher than those of the monolithic A55 (Fig. 6(a); 3.6×10^{-7} S/cm). At 600°C the small bulk arc disappears and only the grain boundary arc, which governs the conduction process, is observed. The conductivity values are 5.5×10^{-4} and 4.3×10^{-4} S/cm for FGM-55 and FGM-45, respectively. At 750°C only a small arc corresponding to electrode/material interface can be detected.

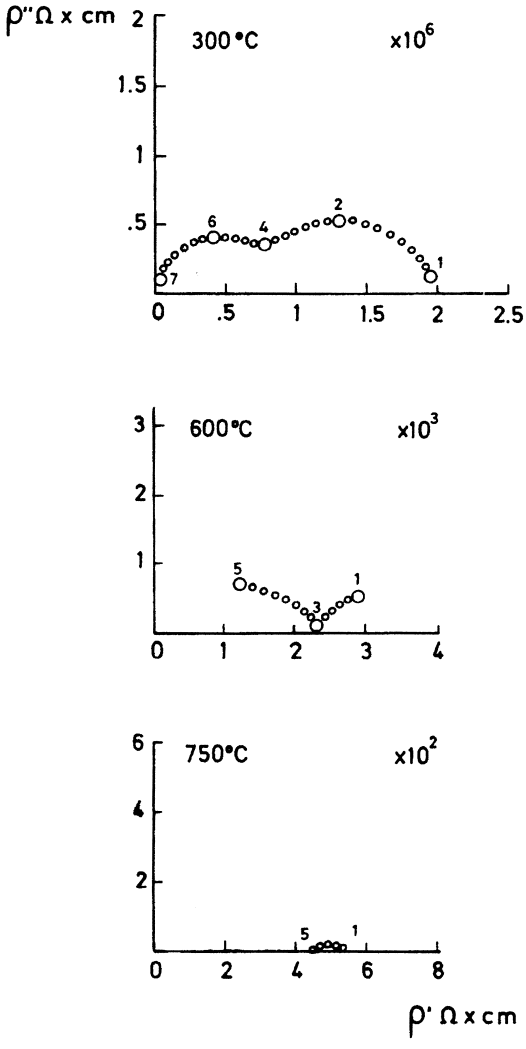

Fig. 7. Impedance spectra of functionally graded materials (FGM)-45 at different temperatures.

Fig. 8 plots the log of total conductivity as a function of reciprocal temperature. The FGMs have higher conductivity in all cases than the related monolithic materials, except in the case of the sample FGM-100, whose conductivity is slightly lower than that of 100A sample. The activation energies of samples FGM-70 and -55 and the corresponding monolithics (70A and 55A) are about 1.20 eV, which is the value mostly accepted for pure TZP materials.

4. Discussion

It is generally accepted that the addition of finely divided alumina particles causes a marked reduction in the chemical diffusivity and, consequently, a decrease in the electrical conductivity.[18] The classical theory of conduction and diffusion in binary mixtures of two compatible phases[18] can be expressed, for a non-conducting spherical secondary phase (i.e. Al_2O_3), as:

$$\sigma_d = (1-f)\sigma_0/(1+0.5f), \quad (1)$$

where f is the volume fraction of particles, σ_0 is the conductivity of the matrix phase, and σ_d is the conductivity of the global composite material.

As can be observed, this theory fits properly some of the results reported in the literature,[20] in which the electrical conductivity response fits well for systems where the microstructural geometry consists of a matrix of either TZP or PSZ (partially stabilized zirconia) and a secondary phase of finely divided alumina particles located at the grain boundaries between the matrix grains. Therefore, Eq. (1) must only be applied in a monolithic material and in each isolated layer into the laminated. In the case of lamellar systems, as those prepared in this work, the FGM microstructural geometry is obtained by the superposition of the parallel layers that have different distributions of the two phases. We assume that in each of the layers there is a homogeneous distribution of the two phases so that the fine secondary phase is also located at the grain boundaries between the matrix grains. The problem at this point concerns the actual composition of each FGM and the possibility to compare them with the corresponding monolithic materials, i.e. the aim is to determine if the total conductivity in the FGMs is governed either by the composition of the last layer (layer with higher alumina content) or by the average composition in the whole FGM. These considerations may allow us to discern which of the two discussed geometries is operating in the conduction process.

Fig. 9 plots the log of total conductivity defined as the reciprocal of the total resistivity (the sum of both bulk and blocking contributions), for (a) all monolithics and (b) FGMs at 750°C. Similar trends are observed for

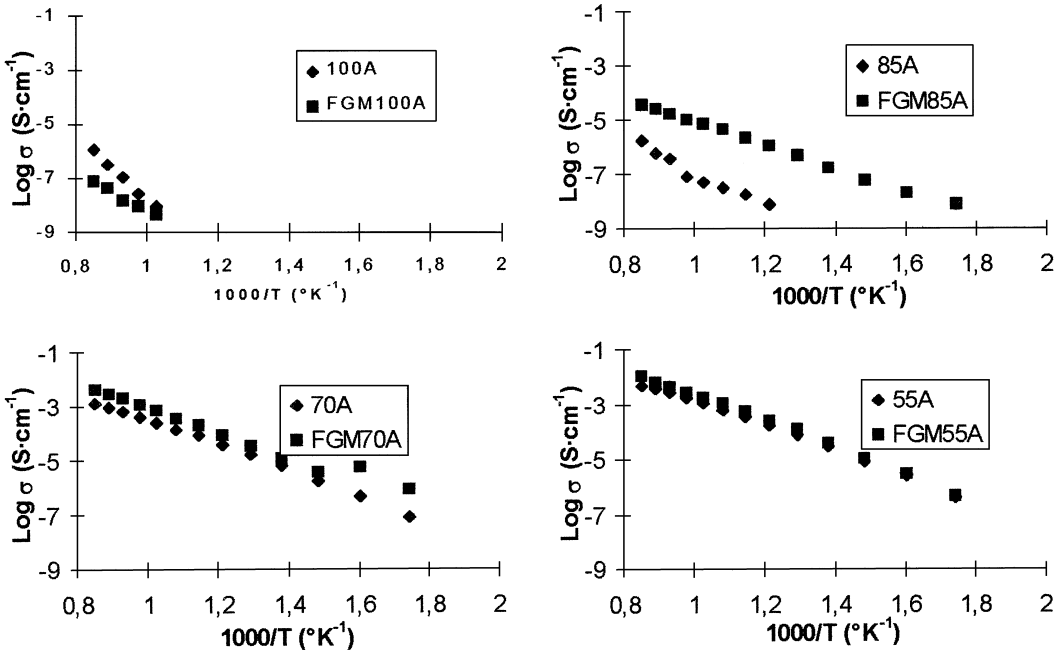

Fig. 8. Plot of the log of total conductivity as a function of reciprocal temperature, comparing some monolithics with the associated functionally graded materials (FGMs).

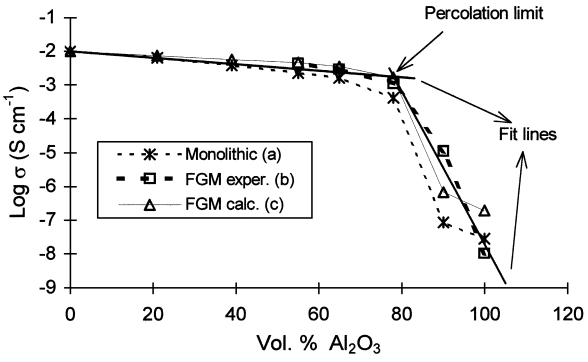

Fig. 9. Log of conductivity as a function of alumina volume fraction for the monolithics, and calculated and experimental values for the functionally graded materials (FGMs) at 750°C. Fit lines have been calculated using the points above and below 80 vol.%.

lower temperatures. Curve "*a*" represents the measured total conductivity of the monolithics for different Al_2O_3 concentrations. Curve "*b*" plots the measured total conductivity of the FGM samples as a function of the Al_2O_3 content in the last layer. It can be seen that conductivity slightly decreases as a function of alumina concentration up to concentrations of 78 vol.% of alumina (70 wt.%), where a dramatic slope change is observed. The curves can be represented as two intercepting straight lines, whose intersection corresponds to the alumina percolation limit, as reported elsewhere.[25] So, in both cases, monolithics and FGMs, the same electrical pattern is registered, thus suggesting that FGMs have a layered structure in which the barrier blocking nature of this kind of interface is not actually predominating from an electrical point of view. Hence, the oxygen vacancy motion is limited only by the blocking effect of alumina particles, following exactly the same trend as a monolithic composite material. In addition to the experimental measurements, the effective medium theory (EMT) was considered for calculating the total resistivity of FGM's. For these calculations, the following equation[24] was used:

$$\rho_d = \Sigma f_i \rho_i \quad (2)$$

being f_i the Al_2O_3 vol. fraction in each layer i, and ρ_i the corresponding resistivity, determined considering the thickness of each layer and its resistivity as measured in the monolithics. The result of this calculation is also plotted in Fig. 9 (curve *c*). Calculated results are in good agreement with the experimental measurements (Fig. 9(b)), so that the EMT can be applied to these composite materials. Table 4 reports the total specific resistivity measured in monolithics and FGMs as well as the resistivity calculated for FGMs using the Eq. (1) (considering the FGM as a monolithic Y-TZP matrix with all the Al_2O_3 homogeously dispersed) and Eq. (2).

The slight differences between the calculated and measured total conductivities for the FGMs below 80 vol.% Al_2O_3 suggest again that the interfaces have no influence on the total electrical response of this kind of material with graded structure. If any electrical interphase exists between layers, the experimental conductivity of the material will decrease much significantly, which is not the case. So it can be concluded that in these layered

Table 4
Total specific resistivity of the monolithic and functionally graded materials (FGMs) at (a) 300 and (b) 750°C[a]

Monolithic		FGM				
Composition (Al_2O_3 vol.%)	Measured	Sample	Measured	Calculated [using Eq. (2)]	Calculated [using Eq. (1)]	Average Al_2O_3 vol.%
(a) 300°C						
100	–	FGM-100	–	–	5.1×10^5	52
90	–	FGM-85	1.5×10^8	–	4.3×10^5	45
78	1.3×10^7	FGM-70	1.2×10^7	2.8×10^6	3.8×10^5	39
65	2.7×10^6	FGM-55	2.3×10^6	1.1×10^6	3.3×10^5	31
55	2.0×10^6	FGM-45	2.0×10^6	7.9×10^5	2.9×10^5	25
39	9.4×10^5	FGM-30		5.1×10^{5b}	2.6×10^{5b}	18
21	4.2×10^5	FGM-15		3.1×10^{5b}	2.2×10^{5b}	9
0	1.9×10^5	FGM-0	1.9×10^5	1.9×10^5	1.9×10^5	0
(b) 750°C						
100	3.7×10^7	FGM-100	10^8	5.3×10^6	2.7×10^2	52
90	1.2×10^7	FGM-85	9.7×10^4	1.5×16^6	2.2×10^2	45
78	2.4×10^3	FGM-70	9.0×10^2	6.0×10^2	2.0×10^2	39
65	6.2×10^2	FGM-55	3.5×10^2	2.8×10^2	1.7×10^2	31
55	4.3×10^2	FGM-45	4.5×10^2	2.2×10^2	1.5×10^2	25
39	2.6×10^2	FGM-30		1.7×10^{2b}	1.3×10^{2b}	18
21	1.5×10^2	FGM-15		1.3×10^{2b}	1.1×10^{2b}	9
0[b]	10^2	FGM-0	10^2	10^2	1.0×10^2	0

[a] Calculations for FGM has been made using Eq. (1) (considering the average amount of alumina in the materials as dispersed in a monolithic material) and Eq. (2).
[b] Calculated values for non-prepared samples.

FGMs, mechanical and compositional interphases exist, but no electrical interfaces can be detected. It is also remarkable that the global composition of the FGM having a 90 vol.% of A in the last layer, corresponds only to a total alumina content in the whole FGM compact of 45 vol.%. But if the conductivity of a monolithic with 45.% vol is compared with the conductivity of the FGM with seven layers the difference is of three orders of magnitude even when both materials have the same global composition.

5. Conclusions

Laminated ceramics with tailored microarchitecture can be designed and prepared by a relatively easy forming method such as sequential slip casting, in which an accurate control of both the composition and the thickness of each layer can be achieved. In such a way, tailor-made FGMs can be designed to modify the electrical response of a monolithic material. In the present work, laminated FGMs of tetragonal zirconia with increasing additions of Al_2O_3 have been studied and compared to monolithic biphasic materials

Most of the observations reported here converge to the conclusion that in the examined FGMs and monolithics, two regimes characterize the alumina blocking process. Up to 80 vol.% alumina a sort of ideal behavior prevails. The composition 80% corresponds to the percolation limit. Above 80 vol.% Al_2O_3 a drift from this behavior sets in and pushes the percolation limit up to about 90%.

In the FGMs there are microstructural interfaces. Usually, reported laminates exhibit a blocking phenomenon corresponding to a thin sheet between layers. In our graded materials it seems that, below the percolation limit, there are no significant electrical interfaces phenomena. When the last layer is alumina, the conduction is governed by this very resistive layer. But as last layer is a layer with at least 15% of ZrO_2-Y_2O_3 the conduction mechanism is governed by the graded distribution of the alumina in the FGM. For laminates graded materials with higher zirconia concentrations in the last layer this assestment is also observed.

The FGM concept can be used for devices in which the control of the oxygen vacancy movement is desirable, and after selecting the optimum components, can also be applied in SOFC, since the introduction of intermediate layers allows the reduction of the expansion coefficient mismatching between the electrode/electrolyte components.

References

1. Yamanouchi, M., Koizumi, M., Hirai, T. and Shiota, I. eds. *Proceedings of the First International Symposium on Functionally Gradient Materials*. FGM Forum, Tokyo, Japan, 1990.
2. Holt, J. B., Koizumi, M., Hirai, T. and Munir, Z. A. eds. Functionally Gradient Materials, *Ceramic Transactions, Vol 34* The American Ceramic Society, Westerville, OH, USA, 1993.

3. Ilschner, B. and Cherradi, N. eds. *Proceedings of the Third International Symposioum on Structural and Functional Gradient Materials*, Presses Polytech. Univ. Romandes, Lausanne, Switzerland, 1995.
4. Sanchez-Herencia, A. J., Materiales Cerámicos con Función Gradiente. *Bol. Soc. Esp. Ceram. Vid.* 1996, 35, 247-256.
5. Hirai, T., Functionally gradient materials. In Materials Science and Technology, A comprehensive treatment, Vol. 17B, Processing of Ceramics, part II, Chapter 20, ed. R.J. Brook, VCH Verlagsgesellschaft, Weinhein, Germany, 1996, pp. 293–341.
6. Zhu, X., Wang, Q. and Meng, Z., A functionally gradient piezoelectric actuator prepared by powder metallurgical process in PNN-PZ-PT system. *J. Mater. Sci. Lett*., 1995, **14**, 516–518.
7. Kawai, T., Miyazaki, S. and Araragi, M., A piezoelectric actuator using functionally gradient material. *Yokogawa Technical Report (English Edition)*, 1992, **14**, 6–10.
8. Eguchi, K., Hoshino, T. and Fujihara, T., Performance analysis of FGM-based direct energy conversion system for space power applications. In *Third International Symposium on Structural Functional Gradient Materials Proceedings of FGM '94*, ed. B. Ilschner and N. Cherradi. Presses Polytech. Univ. Romandes, Lausanne, Switzerland, 1995, pp. 619–625.
9. Niino, M. and Koizumi, M., Projected research on high-efficiency energy conversion materials. In *Third International Symposium on Structural and Functional Gradient Materials Proceedings of FGM '94*, ed. B. Ilschner and N. Cherradi. Presses Polytech. Univ. Romandes, Lausanne, Switzerland, 1995, pp. 601–605.
10. Nagata, M., Iwasawa, C., Yamaoka, S., Seino, Y. and Ono, M., Development of self-supporting air electrode SOFC. In *Proceedings of the Fourth International Symposium on Solid Oxide Fuel Cells (SOFC-V)*, ed. M. Dokiya, O. Yamamoto, H. Tagawa and S. C. Singhal. Pennington, Electrochem. Soc, NJ, USA, 1995, pp. 173–179.
11. Sasaki, K. and Gauckler, L. J., Functional gradient electrode/electrolyte for solid oxide fuel cells: gradient materials design for an electrochemical energy conversion device. In *Third international Symposium on Structural and Functional Gradient Materials*, ed. B. Ilschner and N. Cherradi. Presses Polytech. Univ. Romandes, Lausanne, Switzerland, 1995, pp. 651–656.
12. Sasaki, K., Bohac, P. and Gauckler, L. J., Doped-In_2O_3 as a cathode material for solid oxide fuel cells. In *Proceedings of the Third International Symposium on Solid Oxide Fuel Cells*, ed. S. C. Singhal and H. Iwahara. Pennington, Electrochem. Soc, NJ, USA, 1993, pp. 288–300.
13. Markworth, A. J., Ramesh, K. S. and Parks, W. P. Jr, Review modelling studies applied to functionally gradient materials. *J. Mat. Sci*., 1995, **30**, 2183–2193.
14. Bonanos, N., Steele, B. C. H., Butler, E. P., Johnson, N. B., Worrell, W. L., Macdonald, D. D. and McKubre, M. C. H., Applications of impedance spectroscopy. In Impedance Spectroscopy: Emphasizing Solid Materials and Systems, ed. J. Ross Mc Donald, J. Wiley, NY, USA, 1897, pp. 191–237.
15. Kleitz, M., Dessemond, L. and Steil, M. C., Model of ion-blocking at internal interfaces in zirconias. *Solid State Ionics*, 1995, **75**, 107–115.
16. Dessemond, L., Muccillo, R., Henault, M. and Kleitz, M., Electric conduction-blocking effects of voids and second phases in stabilized zirconia. *Appl. Phys*., 1993, **A57**, 57–60.
17. Kleitz, M. and Steil, M. C., Microstructure blocking effects versus effective medium theories in YSZ. *J. Eur. Ceram. Soc*., 1997, **17**, 819–829.
18. Miyayama, M., Yanagida, H. and Asada, A., Effects of Al_2O_3 additions on resistivity and microstructure of yttria-stabilized zirconia. *Am. Ceram. Soc. Bull*., 1985, **4**, 660–664.
19. Badwal, S. P. S., Bannister, M. J. and Garret, W. G., Oxygen measurements with $SIRO_2$ sensors. *J.Phys. Sci. Instrum*., 1997, **20**, 531–540.
20. Navarro, L. M., Recio, P., Jurado, J. R. and Durán, P., Preparation and properties evaluation of zirconia-based alumina composites as electrolytes for solid oxide fuel cell systems. Part III: mechanical and electrical characterization. *J. Mater. Sci*., 1995, **30**, 1949–1960.
21. Moreno, R., Sanchez-Herencia, A. J. and Moya, J. S., Functionally gradient materials by sequential slip casting: alumina-yttria tetragonal zirconia. In *Ceramic Transactions, vol 34: Functionally Gradient Materials*, ed. B. Holt, M. Koizumi, T. Hirai and Z. A. Munir. The American Ceramic Society, Westerville, OH, USA, 1993, pp. 145–156.
22. Boukamp, B. A., *EQUIVCRT Software*. University of Twente, Enschede, Netherlands, 1993.
23. Kleitz, M. and Petitbon, F., Optimized SOFC electrode microstructure. *Solid State Ionics*, 1996, **92**, 65–74.
24. Crosbie, G. M., Chemical diffusivity and electrical conductivity in TiO_2 containing a submicron dispersion of SiO_2. *J. Solid State Chem*., 1978, **25**, 367–378.
25. Steil, M. C., Thévenot, F., Dessemond, L. and Kleitz, M., Impedance spectroscopy analysis of conduction percolation in zirconia-alumina composites. In *Third Euro-Ceramics, vol.2*, ed. P. Fernández, J. F. Fernández and S. L. Faenza Editrice Iberica. Castellón de la Plana, Spain, 1993, pp. 271–280.